HIGH-GRADIENT RADIOFREQUENCY PHOTOINJECTOR WITH A DETACHABLE CATHODE ASSEMBLY

I. Shalaby*, L. Malin, M. Holl, S. Karkare, S. G. Tantawi
Arizona State University, Tempe, AZ, USA

Abstract

We present an RF photoinjector architecture that utilizes the TM_{02} mode in the first half-cell housing the cathode. Unlike the conventional TM_{01} mode configuration, this design introduces a controlled discontinuity in the surface field, producing a region free of surface currents. This unique topology allows the cathode to be mechanically separated from the gun body without compromising RF performance or requiring precise electrical continuity at the interface. The photoinjector should, in principle, deliver a very high cathode gradient and, consequently, high beam brightness. At the same time, the detachable cathode assembly is compatible with load-lock systems, which can transfer high QE semiconductor cathodes into high-gradient RF photoinjector structures under UHV.

INTRODUCTION

High-energy electron beams have provided an immense utility in various applications in research, such as X-ray generation [1] and ultrafast electron diffraction (UED) [2, 3], and in industrial applications, such as semiconductor metrology [4, 5] and medical treatment [6, 7]. Following electrons creation from a cathode surface through a photoelectric process, electrons are typically accelerated to relativistic energies (tens of MeVs), using high-gradient RF (~120 MV/m) fed into the photoinjector cavities. Acceleration upon creation is critical for minimizing emittance growth and producing high-brightness electron beams, highlighting the vitality of photoinjector assemblies.

TM_{01} VS TM_{02} DESIGNS

While TM_{01} is the minimalist mode of operation for photoinjector cavities design, multiple issues can emerge due to high RF fields on the metallic surface. For instance, imperfect brazing process of the cathode surface can lead to discontinuities and breakdowns, as well as cavity detuning beyond a reasonable range of the mechanical tuning pins. Significant damage to the cathode surface can inevitably leads to disposal of the entire photoinjector assembly. Moreover, the TM_{01}-mode design is inherently incompatible with semiconductor cathodes, which provide high QE, as they require growth and transfer under UHV. In this work, we present an alternative mode of operation, TM_{02}, for the cathode cavity which completely avoid brazing complications by using a braze-free cathode plug. This standalone cathode plug provides a soft tuning knob for the cathode cavity using precise positioning of the cathode plug. The detachable plug can be easily replaced, if damaged, and can also host semiconductor cathodes via a load-lock system.

* isshalab@asu.edu

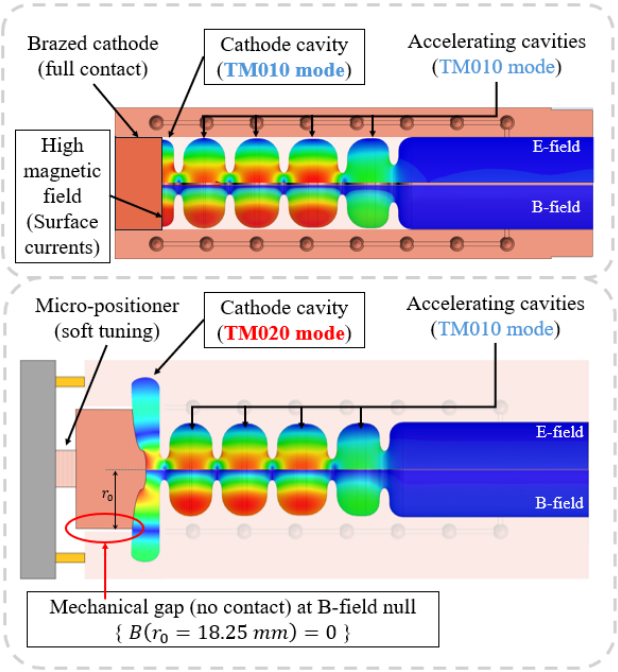

Figure 1: Comparison between TM_{01} amd TM_{02} designs for the first cathode cavity of a photoinjector assembly.

As shown in Fig. 1, designing a standalone cathode plug is feasible, in the TM_{02}-mode, by exploiting a magnetic field null on the metallic surface where surface currents are eliminated and a mechanical gap can be implemented without breakdown risks. This gap allows for a free-standing cathode which can be precisely positioned for tuning, easily replaceable, and can be integrated into a larger vacuum assembly for semiconductor cathodes integration.

CAVITY DESIGN OPTIMIZATION

To reach an optimal cavity design, it is necessary to strike a balance between the acceleration voltage V_{acc} and power losses on the metallic walls P_{loss} due to surface currents. Shunt impedance ($R_{\mathrm{s}} = |V_{\mathrm{acc}}|^2/P_{\mathrm{loss}}$) is the figure of merit used to evaluate and optimize cavity performance. Power loss is calculated using ($P_{\mathrm{loss}} = \frac{1}{2\delta\sigma}\oiint_S |H_{\parallel}|^2\, da$), where $H_{\parallel}$ is the surface magnetic field, δ is the skin depth, and σ is the conductivity. On the other hand, the acceleration voltage is calculated using the on-axis electric field E_z. Since electrons reach relativistic speeds fairly quickly under high gradient RF, a Lagrangian formalism is used for a single electron in a linear electric field E_z. This results in two transcendental equations $\{\partial\gamma/\partial z = (e/m_e c)|E(z)|e^{i(\omega t+\phi)}$, $\partial t/\partial z =$

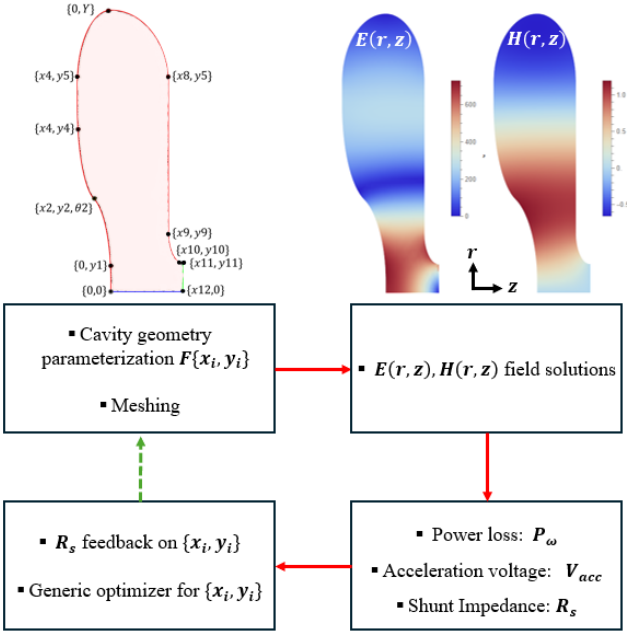

Figure 2: Iterative process for cavity design optimization [8].

$\gamma/c\sqrt{\gamma^2-1}\}$ which can be solved numerically to obtain the final acceleration voltage and optimal injection phase ϕ. where ω=2πf, (in our case, f= 9.3 GHz). The acceleration voltage can be calculated as $V_{\rm acc} = (\gamma - 1) * m_e c^2/e$.

As shown in Fig. 2, the cavity geometry is parametrized using a set of coordinate points connected by ellipses and straight lines [8]. A 2D mesh (assuming azimuthal symmetry) is applied and Maxwell's equations are solved numerically for this geometry with appropriate boundary conditions. Once fields are obtained, Acceleration voltage, power loss, and shunt impedance are then calculated. A generic optimizer is used on cavity parameters $\{x_i, y_i\}$ to iteratively search for optimal geometry that maximizes shunt impedance.

BENCHMARK RESULTS

During the optimization process, the on-axis cavity width is kept fixed at 5.5 mm (0.34 $\lambda_{\rm RF}/2$) where −50° is the optimal injection angle ϕ for both modes. With 120 MV/m acceleration gradient in the first cavity, both $\rm TM_{01}$ and $\rm TM_{02}$ designs are simulated and key benchmark results are listed in Table 1. While the $\rm TM_{01}$ design shows a slightly higher acceleration voltage $V_{\rm acc}$ under the same acceleration gradient, the $\rm TM_{02}$ design utilizes RF power more efficiently with smaller power losses $P_{\rm loss}$ on the cavity walls, resulting in a higher shunt impedance $R_{\rm s}$ for the $\rm TM_{02}$ design. This RF power utilization is also apparent in the field ratio $E_{\rm max}/E_{\rm acc}$ between the maximum field on the surface and the on-axis field at the cathode. Results shows maximum surface E-field is 10% higher in the $\rm TM_{01}$ design while only 6% higher in the $\rm TM_{02}$ case. Note that geometric optimization is only applied to the TM_{02} design and compared with a conventional $\rm TM_{01}$ design.

Table 1: Benchmark results for 120 MV/m acceleration gradient in the cathode cavity.

Results	**$\rm TM_{01}$**	**$\rm TM_{02}$**
Inj. phase ϕ [deg]	−50°	−50°
γ	1.835	1.775
$V_{\rm acc}$ [kV]	426.8	395.9
$P_{\rm loss}$ [kW]	668	561.5
$R_{\rm s}$ [kΩ]	**272.7**	**278**
$E_{\rm max}/E_{\rm acc}$	1.1	1.06

After cathode cavity optimization in the $\rm TM_{02}$ mode, a full 4.5-cell assembly is constructed by integrating the new cathode cavity with additional four acceleration cavities operating in the $\rm TM_{01}$ mode, as shown in Fig. 1. The cavities' radii, along with the in-coupling aperture radius, are fine-tuned in HFSS to critically couple RF power and maintain an equal on-axis E_z field strength among first 3.5 cavities. The field strength in the last (most right) cavity is weaker due to the wider in-coupling aperture. Figure 3 (A) shows the S_{11} parameter showing five modes (0, $\pi/4$, $\pi/2$, $3\pi/4$, π) of the full photoinjector assembly, where the π-mode is critically coupled with $S_{11,\pi} \sim -50$ dB at 9.3 GHz. Figure 3 (B) shows the on-axis E_z field strength (black) and phase (orange), inside the full photoinjector assembly, for the π-mode.

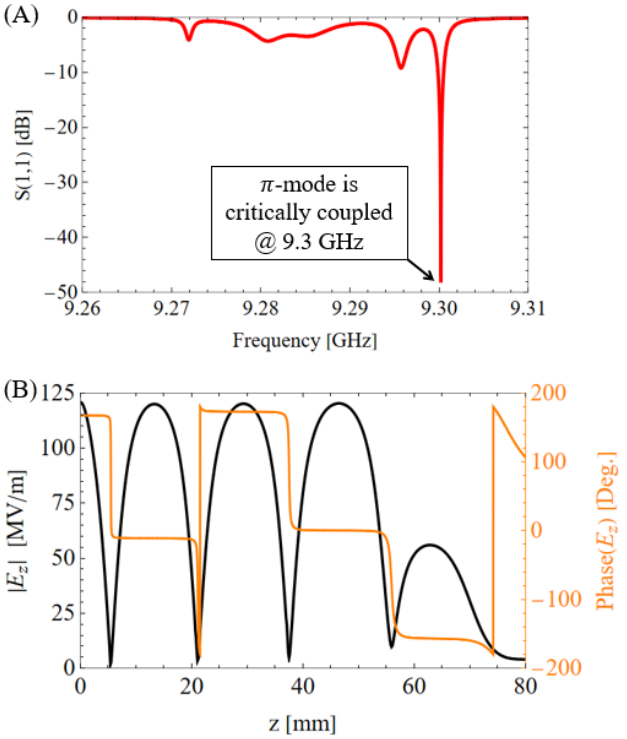

Figure 3: (A) Coupling strength (S_{11}) of the 4.5-cell photoinjector assembly with cathode cavity in the $\rm TM_{02}$ mode. (B) On-axis E_z field strength (black) and Phase (orange) for the critically-coupled π mode at 9.3 GHz.

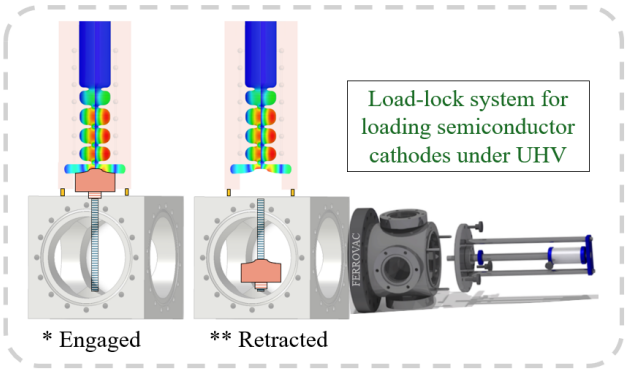

Figure 4: Schematic for the integration of semiconductor cathodes into high-gradient RF cavities using detachable cathode plugs.

DETACHABLE CATHODE DESIGN

The TM_{02} mode, with a region free of surface currents, allows the design of a mechanical gap between the cathode plug and photoinjector assembly. Such design permits standalone cathodes to be used in high-gradient RF cavities, avoiding brazing complications. Precise positioning of the cathode plug allows for soft tuning of the cathode cavity which avoids complications that results from aggressive mechanical tuning. Additionally, a replaceable plug design allows pushing RF fields to even higher gradients without risking disposal of the entire photoinjector assembly.

On the other hand, this detachable cathode design provides a blueprint for integrating semiconductor cathodes, with high quantum efficiency, into high-gradient RF systems. This integration has been challenging, for fully-brazed photoinjectors, as semiconductor cathode require growth and transport under UHV. Figure 4 provides a schematic for this integration where semiconductor cathodes can be grown, in-situ or transported in a vacuum suitcase, and inserted into a load-lock system under UHV. The cathode plug can then be retracted into a vacuum chamber where semiconductor cathodes can be transferred to the plug using the load-lock system. The cathode plug can then be engaged back, using a translation stage, into the photoinjector assembly for high-gradient RF operations.

CONCLUSION AND FUTURE WORK

The use of free-standing cathode plugs, by implementing the TM_{02} cathode cavity design, in high-gradient RF photoinjectors avoids brazing complications and provides an additional tuning knob of the cathode cavity. The risk of cathode surface damage under higher RF gradients is more acceptable with a replaceable plug assembly. This design also lays out a framework for integrating semiconductor cathodes into high-gradient RF photoinjectors. A more holistic geometry optimization, for the cathode cavity design, will include the on-axis cavity width and the cathode surface curvature to mutually optimize bunch emittance along with shunt impedance.

REFERENCES

[1] W. S. Graves *et al.*, "Compact x-ray source based on burst-mode inverse Compton scattering at 100 kHz", *Phys. Rev. ST Accel. Beams*, vol. 17, no. 12, p. 120701, 2014. doi:10.1103/PhysRevSTAB.17.120701

[2] P. Musumeci, J. T. Moody, C. M. Scoby, M. S. Gutierrez, H. A. Bender, and N. S. Wilcox, "High quality single shot diffraction patterns using ultrashort megaelectron volt electron beams from a radio frequency photoinjector", *Rev. Sci. Instrum.*, vol. 81, no. 1, p. 013306, 2010. doi:10.1063/1.3292683

[3] S. P. Weathersby, G. Brown, M. Centurion, *et al.*, "Mega-electron-volt ultrafast electron diffraction at SLAC national accelerator laboratory", *Rev. Sci. Instrum.*, vol. 86, no. 7, p. 073702, 2015. doi:10.1063/1.4926994

[4] N. G. Orji *et al.*, "Metrology for the next generation of semiconductor devices", *Nat. Electron.*, vol. 1, no. 10, pp. 532–547, 2018. doi:10.1038/s41928-018-0150-9

[5] K. Nakamae, "Electron microscopy in semiconductor inspection", *Meas. Sci. Technol.*, vol. 32, no. 5, p. 052003, 2021. doi:10.1088/1361-6501/abd96d

[6] K. R. Hogstrom and P. R. Almond, "Review of electron beam therapy physics", *Phys. Med. Biol.*, vol. 51, no. 13, R455–R489, 2006. doi:10.1088/0031-9155/51/13/R25

[7] P. G. Maxim, S. G. Tantawi, and B. W. Loo, "PHASER: a platform for clinical translation of FLASH cancer radiotherapy", *Radiother. Oncol.*, vol. 139, pp. 28–33, 2019. doi:10.1016/j.radonc.2019.05.005

[8] M. H. Nasr and S. G. Tantawi, "New geometrical-optimization approach using splines for enhanced accelerator cavities' performance", in *Proc. IPAC'18*, Vancouver, BC, Canada, pp. 4395–4397, Jun. 2018. doi:10.18429/JACoW-IPAC2018-THPMK049